JOURNAL OF GUIDANCE, CONTROL, AND DYNAMICS
Vol. 20, No. 6, November–December 1997

Optimum Mission Performance and Multivariable Flight Guidance for Airbreathing Launch Vehicles

David K. Schmidt*
University of Maryland, College Park, Maryland 20742-3200

The optimum mission performance is addressed, and a simple, robust, multivariable flight-guidance law for following the prescribed optimum trajectory of an airbreathing, single-stage-to-orbit launch vehicle is proposed. Discussion focuses on the critical scramjet-powered phase of flight for a hydrogen-fueled vehicle. The performance analysis, based on energy-state arguments, suggests that, whereas station keeping and orbital maneuvers will clearly require rocket propulsion, low-Earth-orbital energy can be achieved with scramjet propulsion. The feedback guidance law for trajectory following is also synthesized using total-energy concepts, along with an approach consistent with quantitative feedback theory. The open-loop system in the guidance analysis is multivariable, unstable, and nonminimum phase. Furthermore, the vehicle characteristics lead to significant interactions between the inputs and responses. The guidance law developed relies on an integrated flight- and propulsion-control inner loop to stabilize the attitude dynamics and regulate the engine performance. It is shown that this hierarchical integrated synthesis technique yields simple, classical-looking compensation that robustly stabilizes the system and delivers very good performance.

Introduction

TO reduce the costs of delivering payload to orbit, achieving low Earth orbit (LEO) with a single-stage vehicle has been proposed. Such a vehicle must transit from launch to Mach 25 at an altitude of about 200,000 ft. Airbreathing propulsion is considered, which implies that the vehicle would be operated in the atmosphere over a much greater portion of the trajectory than would be the case with rocket propulsion. To maximize payload to orbit, trajectory optimization and guidance will be important.

Formal studies of the optimization of such launch trajectories have been previously reported by several authors, including Corbin et al.,[1] Van Buren and Mease,[2] Ardema et al.,[3] and Sachs et al.[4] In all of these studies, numerical trajectory-optimization techniques were employed, and the dynamic model was limited to the point-mass model of the vehicle. In most of these studies, the three-degree-of-freedom equations of motion were enforced along the trajectory, whereas in Ref. 2 the singular-perturbation decomposition was utilized. In the work reported here and elsewhere,[5,6] we have employed the classical energy-state approach,[7] which admits an approximate graphical solution to the optimization problem. We have previously shown both that this method can be justified for this class of vehicle and that results obtained using the energy-state approach can agree quite favorably with results obtained via more sophisticated techniques. Also, the simple energy-state concept aids considerably in understanding the characteristics of the system.

But determination of the optimal trajectory is not the only issue under study here. For these vehicles, a highly integrated guidance and control system will be necessary to achieve the requisite system performance and stability robustness.[8] This is because the unstable airframe, propulsion system, and structural dynamics are highly interactive. And in those studies noted previously in which guidance laws were discussed, the attitude dynamics were ignored.

In this paper we will both describe the scramjet-powered phase of an optimum flight profile for a generic airbreathing vehicle and put forth an integrated, multivariable flight guidance and control feedback law. This guidance law is intuitive, extremely simple in form, and consistent with the energy-state concepts so useful in the trajectory analysis. Again, the attitude dynamics have not been ignored in this investigation. But the use of a multivariable integrated flight and propulsion inner-loop control system reported previously[8] is treated specifically, leading to a natural hierarchical guidance and control structure.

Received Nov. 21, 1996; presented as Paper 97-0458 at the AIAA 35th Aerospace Sciences Meeting, Reno, NV, Jan. 6–9, 1997; revision received April 1, 1997; accepted for publication April 5, 1997.

*Professor and Director, Flight Dynamics and Control Laboratory. Associate Fellow AIAA.

Vehicle Characteristics

The class of vehicle being considered is shown schematically in Fig. 1. The geometry is generic but was selected to reflect key characteristics of the X-30 National Aerospace Plane vehicle. The configuration is a lifting body, consisting of a forebody/engine inlet, internal scramjet engine module, and afterbody/exhaust nozzle. The study configuration is 150 ft in length, with a weight at scramjet ignition taken to be 300,000 lb. A performance model for the vehicle and propulsion system is described in more detail in Refs. 9 and 10.

This vehicle configuration has two important characteristics: the vehicle's forebody performs a significant part of the inlet compression process, and its afterbody constitutes a large part of the nozzle. The engine design thus encompasses the entire undersurface of the vehicle, and the engine and airframe become one. The vehicle's lower forebody surface produces aerodynamic lift, in addition to providing a precompression surface upstream of the engine inlet. The afterbody/nozzle surface experiences exhaust-plume impingement, which produces both propulsive thrust and lift.

More specifically, again with reference to Fig. 1, the propulsive forces and total available lift are

$$F_x = Th_{\text{engine}} + X_{\text{plume}} + X_{\text{turn}}, \qquad F_z = Z_{\text{plume}} + Z_{\text{turn}}$$

$$L_{\text{avail}} = L_{\text{aero}} + F_x \sin(\alpha) - F_z \cos(\alpha)$$

whereas the available thrust along the velocity vector is

$$Th_{\text{avail}} = F_x \cos\alpha + F_z \sin\alpha \tag{1}$$

Figure 2 shows the scramjet's specific impulse (at a velocity of 10,000 ft/s) as a function of the vehicle's angle of attack and altitude, where the specific impulse is

$$I_{\text{sp}} \equiv \frac{Th_{\text{avail}}}{\dot{W}_{\text{fuel}}} = \frac{F_x \cos\alpha + F_z \sin\alpha}{\dot{W}_{\text{fuel}}} \tag{2}$$

Note the highly interactive nature of the forces on the vehicle and the propulsion system's performance. Specifically, the aerodynamic and propulsive lift and axial forces and the specific impulse are all strongly dependent on vehicle angle of attack, flight velocity, and altitude.

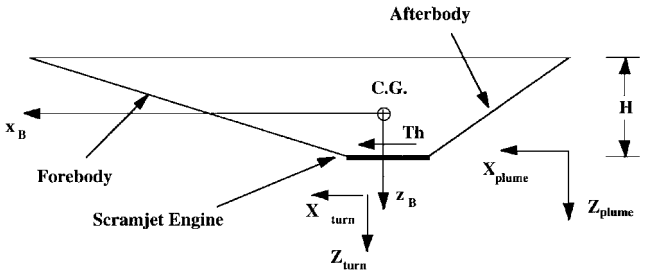

Fig. 1 Generic hypersonic single-stage-to-orbit (SSTO) configuration, side view.

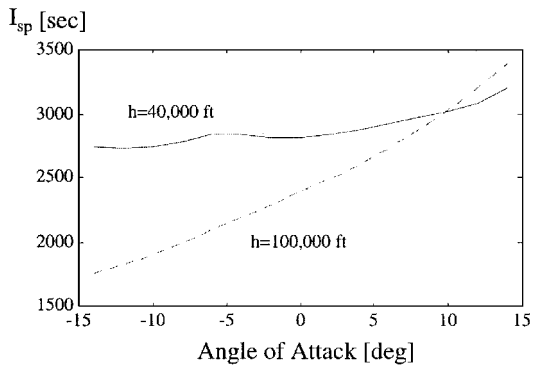

Fig. 2 Scramjet specific fuel consumption, Mach = 10.

Optimum Ascent Trajectory

The mission considered is payload insertion into LEO. In investigating the flight performance, primary interest will be on the unique scramjet-powered phase of flight. This phase is of special interest because it is critical if airbreathing propulsion is to have promise for this mission. It is also the phase of flight about which the least is known.

The scramjet-powered phase would be initiated after the vehicle is first accelerated via a somewhat more traditional propulsive device such as a turboramjet. The scramjet-powered phase would then ultimately terminate after conversion to chemical rocket propulsion. One issue to be addressed is the condition for optimum switching from turboramjet to scramjet and from scramjet to rocket.

For the mission in question, a critical performance metric is maximum orbital payload and, therefore, the minimum-fuel trajectory is of primary significance. For the purpose of the discussion that follows, consider the flight to be restricted to a vertical plane. The potential plus kinetic energy per unit weight at sea level, or energy height, is

$$E = \frac{hR_0}{R_0 + h} + \frac{0.5V^2}{g_0}$$

where R_0 is the radius of the Earth. Under energy-state assumptions,[6] planar flight over a spherical, nonrotating Earth is primarily governed by the relation

$$\frac{\mathrm{d}E}{\mathrm{d}W_{\text{fuel}}} = \frac{\dot{E}}{\dot{W}_{\text{fuel}}} = \frac{V}{\dot{W}_{\text{fuel}}}\left(\frac{Th_{\text{avail}} - D_{\text{aero}}}{W}\right) \tag{3}$$

or, equivalently,

$$\frac{\mathrm{d}E}{\mathrm{d}W_{\text{fuel}}} = \frac{VI_{\text{sp}}}{W}\left(1 - \frac{D_{\text{aero}}}{Th_{\text{avail}}}\right)$$

and the objective function to be minimized is

$$W_{\text{total fuel}} = \int_{t_0}^{t_f} \dot{W}_{\text{fuel}}\,\mathrm{d}t = \int_{E_0}^{E_f} \frac{\mathrm{d}E}{\mathrm{d}E/\mathrm{d}W_{\text{fuel}}} \tag{4}$$

The solution algorithm to find the minimum-fuel ascent trajectory is the familiar one, as follows.

At each energy level E, operate the vehicle so as to maximize

$$\frac{\mathrm{d}E}{\mathrm{d}W_{\text{fuel}}} \tag{5}$$

and global minimization of the fuel is found by locally maximizing $\mathrm{d}E/\mathrm{d}W_{\text{fuel}}$.

Note at this point that the system variables, along with their functional dependence, are

$$E = \frac{hR_0}{R_0 + h} + \frac{0.5V^2}{g_0}, \qquad V = V(h, E)$$

$$I_{\text{sp}} = I_{\text{sp}}(\alpha, h, \dot{w}_f, V), \qquad W(h) = W_{\text{initial}} - W_{\text{fuel}}(h)$$

$$D_{\text{aero}} = D_{\text{aero}}(\alpha, h, V), \qquad T_{\text{avail}} = T_{\text{avail}}(\alpha, h, \dot{w}_f, V)$$

$$\dot{w}_f = \text{fuel flow rate}$$

In this performance analysis, the control (decision) variables are propulsive mode (rocket, scramjet, etc.), angle of attack, altitude, and fuel flow rate, with the single state E. Typically, the angle of attack is selected such that vertical equilibrium is enforced, based on some selected vehicle weight W_0. The governing relation is

$$L_{\text{avail}} = L_{\text{aero}} + F_x \sin(\alpha) - F_z \cos(\alpha) = W_0\left[1 - \left(V^2/g_0R\right)\right] \tag{6}$$

As a first observation, if the available lift is assumed approximately equal to the weight (ignoring for the moment the centrifugal acceleration), Eq. (3) may be approximately written as

$$\frac{\mathrm{d}E}{\mathrm{d}W_{\text{fuel}}} \approx \frac{VI_{\text{sp}}}{W}\left(1 - \frac{W}{T_{\text{avail}}}\frac{D_{\text{aero}}}{L_{\text{avail}}}\right)$$

and the dependence on effective L/D and T/W become readily apparent. To gain specific energy, the product of these two quantities must be greater than unity rather than, for example, requiring T/W to exceed unity. Also observe that maximizing L/D alone can only yield a performance payoff if it does not come at the expense of T/W and I_{sp}. Given the interactive nature of these vehicles, this is not likely. Finally, again recall that L_{avail} here includes both aerodynamic and propulsive effects.

Now consider the question of optimum propulsion mode switching. We see from the solution algorithm (5) that the optimum propulsion mode at a particular flight condition (V and h) is simply that which delivers the maximum $\mathrm{d}E/W_{\text{fuel}}$. And from Eqs. (2) and (3), the significance of I_{sp} in this regard is readily apparent. Assume, for example, that the available thrust achievable at some particular flight condition (V and h) is the same for any candidate propulsion system (ramjet, scramjet, rocket). Then the optimum propulsion mode at that flight condition is simply that which delivers the highest I_{sp}. If on the other hand, available thrust was not the same for all propulsion modes, the complete right-hand side of Eq. (3) must be evaluated (maximized) to determine the optimum mode. (In Ref. 2 the concept of effective I_{sp} was introduced. But the basic idea is identical to the discussion here.)

Observe from the propulsion characteristics given in Ref. 1, for example, that at flight Mach numbers below about 5–6 in the atmosphere, the ramjet will have superior I_{sp}, whereas above this Mach number the scramjet delivers superior I_{sp}. Further, at higher altitudes and Mach numbers ($M = 20$–25 and $h = 200{,}000$–$250{,}000$ ft), the rocket I_{sp} will be superior. Based on this argument, it appears that the scramjet is then optimal for flight above Mach 5–6, until almost achieving orbital conditions. The rocket would then ultimately be required for final orbit insertion and orbit station keeping. All of this would appear to be consistent with the results in Ref. 1, for example, obtained via nonlinear programming.

Consider now the scramjet-powered flight phase in more detail. In particular, assume the scramjet is ignited at $M = 6$, at an altitude chosen arbitrarily for now to be $h = 40{,}000$ ft. This corresponds to an initial specific energy of $E_0 = 600{,}000$ ft. The final specific energy required corresponds to LEO conditions, e.g., $h = 200{,}000$ ft and $V = 25{,}000$ ft/s, or $E_f = 9.9 \times 10^6$ ft. Furthermore, we will assume that the rocket I_{sp} is such that the scramjet is the optimum

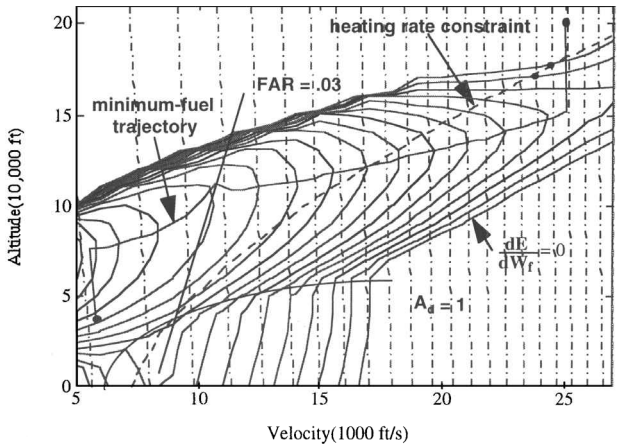

Fig. 3 Energy-gain contours and minimum-fuel trajectory.

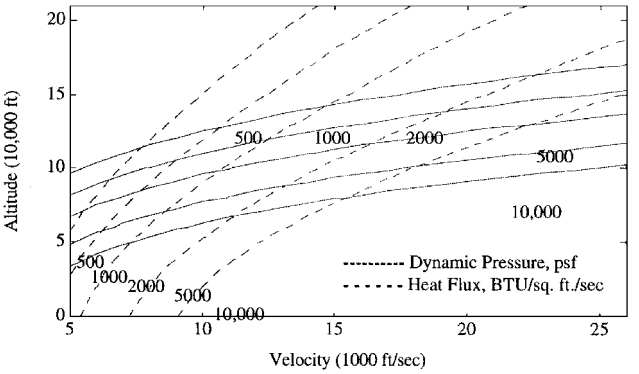

Fig. 4 Constraint boundaries.

mode up to the specified terminal energy. Let the angle of attack be chosen based on Eq. (6), with W_0 taken to be half the ignition weight, or 150,000 lb.

To describe the mission profile for optimal transition between this initial and final energy, consider the data in Fig. 3. The contours of constant dE/dW_{fuel} are shown along with (almost vertical) contours of constant energy E. At each flight condition, the angle of attack was selected to achieve vertical-acceleration equilibrium, and the remaining control variables were selected to maximize dE/dW_{fuel}. The outermost contour, for which dE/dW_{fuel} is zero, therefore defines the flight envelope of the vehicle. Inside this envelope, indefinite sustained flight is theoretically possible.

The optimal altitude/velocity profile, obtained from algorithm (5), is also shown in Fig. 3. Because of the characteristic shape of the contours of energy-gain efficiency ($\dot{E}/\dot{W}_{fuel}$), the optimal trajectory follows the altitude/Mach path of constant-energy until reaching approximately 70,000 ft. At this flight condition, the $\dot{E}/\dot{W}_{fuel}$ reaches its maximum at this energy level. The trajectory then follows a shallow accelerating climb, with almost constant dynamic pressure of 2000 psf, until reaching the final energy level. During this climb phase, the vehicle continues to operate at maximum $\dot{E}/\dot{W}_{fuel}$ at each energy level. Finally, a constant-energy climb to 200,000-ft altitude completes the ascent.

For this trajectory, the total fuel required is estimated to be 160,000 lb, with a time of flight of about 1100 s, assuming an initial vehicle weight at scramjet ignition of 300,000 lb. This corresponds to 53% of the ignition weight consumed, and the total weight delivered to orbit insertion (payload plus inert plus additional fuel) is 140,000 lb. These values are very close to those obtained in Ref. 1 for the same mission and similar propulsion characteristics.

Note finally that Fig. 3 suggests that the final energy at LEO can be achieved with scramjet propulsion, although the final orbit insertion point is actually outside the flight envelope of the scramjet-powered vehicle. This means that flight at $M = 25$ and $h = 200{,}000$ ft cannot be maintained indefinitely, which, of course, is true because eventually the orbit will decay unless reboost occurs. Hence station keeping and maneuvering in orbit must be accomplished with rocket propulsion. This result is also compatible with that in Ref. 1, where rocket propulsion was only used at the final orbital insertion.

Consider now the contours plotted in Fig. 4, indicating constant dynamic pressure and stagnation heat flux. This plot should be visualized as overlaid on Fig. 3. By comparing the shape of the contours in Fig. 4 with the optimal trajectory in Fig. 3, the effect of heating or dynamic-pressure constraints can be observed by inspection. If the unconstrained trajectory violates any constraint boundary, the constrained optimal trajectory would lie along the boundary so violated. This is consistent with the optimality criteria (5) and the shape of the contours of constant dE/dW_{fuel} in Fig. 3.

Finally, some of the important time histories along the minimum-fuel trajectory are shown in Fig. 5. Note that the angle of attack and flight-path angle are modest and the Mach in the combustor remains between 1^+ and 4.3. The axial accelerations are greatest initially, approaching 5 g at about 30 s after scramjet ignition.

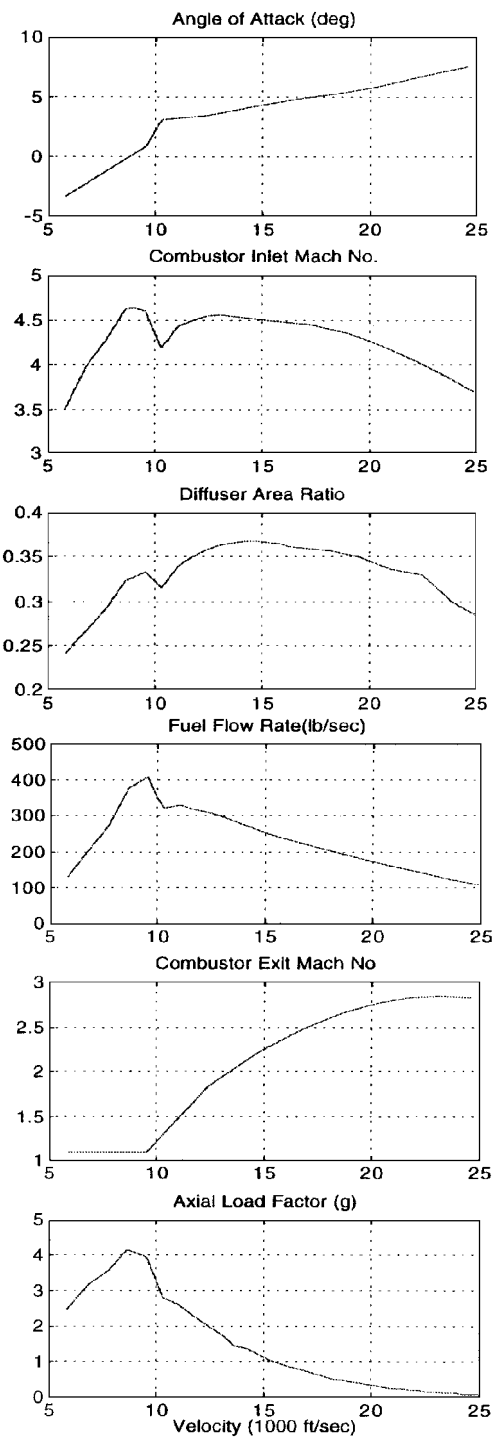

Fig. 5 Selected time histories along minimum-fuel trajectory.

Feedback Guidance Law Development

Attention is now turned to the development of a multivariable closed-loop guidance law for following the prescribed trajectory. The assumptions made at this point are that mission performance will be practically (although perhaps not strictly mathematically) optimal if a predefined minimum-fuel flight path can be followed in the presence of anomalies, such as thrust misalignments and winds; that the guidance laws must deliver a robustly stable closed-loop system; and that guidance-law simplicity is of value.

The approach that we will pursue draws from the total-energy-control (TECS) concept of Lambregts[11] and parallels multivariable quantitative feedback theory (QFT).[12,13] The synthesis technique put forth will deliver path following by regulating altitude and velocity errors relative to the nominal, i.e., optimal, flight profile. Furthermore, although a complete multivariable stability robustness analysis will not be presented, the synthesis approach to be used has been shown to deliver robustly stable multiloop systems.

Finally, in the synthesis of the guidance laws, an inner-loop, integrated flight/propulsion/structural-mode control system is assumed in place. This critical inner-loop control system delivers attitude stabilization, regulation of the combustor flow conditions, and active structural-mode damping. It was discussed fully in Ref. 8. In all analysis to follow, this stability-augmentation system (shown in Fig. 6) is present, and the dynamics include the full position and attitude degrees of freedom. The combustor inlet pressure P_2 is regulated using a variable diffuser area ratio A_d, whereas the engine thrust is regulated using fuel flow $\mathrm{d}m_f/\mathrm{d}t$. The attitude is stabilized and the first structural mode is actively damped by feeding back outputs from a forward (q_f) and an aft (q_a) rate gyro, plus vertical accelerometer, to the pitch control surface δ.

Next, guidance loops will be closed around the system in Fig. 6. The two inputs to be used are the commanded engine thrust Th_c and pitch control surface δ_c. The commanded combustor pressure remains fixed at 1 atm, to maintain the desired combustor-inlet conditions. The main issues that now must be addressed are, first, the selection of the best responses for feedback in this part of the guidance law and, second, the synthesis of the required compensation in these feedback loops.

The significance of the first issue cannot be overemphasized. In fact, Ref. 14 states in relation to the QFT synthesis technique, "... success... may depend on finding the best pairing of plant inputs with outputs." With regard to this issue, the TECS[11] concept has been shown to be effective for the synthesis of integrated, outer-loop flight and propulsion control for path guidance of commercial transport aircraft. In TECS, the two controlled responses are total energy E and altitude h, and of course this is completely compatible with the energy-state concepts used earlier in the discussion of flight-path optimization. The two control inputs are propulsive thrust and angle of attack, or equivalently, thrust and aerodynamic pitch-control surface. This selection of controls and responses naturally follows from the two equations governing energy and flight-path angle γ, which is proportional to climb rate. Namely,

$$\begin{aligned} \dot{E} &= (V/W)[Th_{\text{avail}} - D_{\text{aero}}] \\ V\dot{\gamma} &= (g/W)L_{\text{avail}} - g\cos\gamma + (V^2/R)\cos\gamma \end{aligned} \tag{7}$$

For conventional aircraft, pitch-control-surface (elevator) deflection alone produces little change in drag coefficient from the trim value, and engine thrust is relatively independent of vehicle angle of attack. Therefore, the first of the two preceding expressions suggests that $\dot{E}$ is essentially controlled by thrust, whereas the second suggests that $\dot{\gamma}$ is essentially controlled by aircraft angle of attack, which in the short term is controlled by pitch control surface. Based on these arguments, guidance-law design via conventional TECS involves designing control loops around the 2×2 system

$$y(s) = G(s)u(s)$$

where

$$y = \begin{bmatrix} \dot{E}/V = (\dot{V}/g) + \gamma \\ \dot{ED}/V = (\dot{V}/g) - \gamma \end{bmatrix} \quad \text{and} \quad u = \begin{bmatrix} Th_c \\ \delta_c \end{bmatrix} \tag{8}$$

followed by closing additional outer loops on energy E and altitude h. In the preceding $G(s)$, ED is energy distribution or kinetic minus potential energy.

However, this conventional approach is not appropriate for hypersonic launch vehicles. Three key reasons are as follows. The energy and flight-path responses from engine thrust and pitch control surface are highly coupled, the energy is dominated by the velocity (kinetic energy), and the flight-path response of these vehicles is problematic.

The strong dynamic coupling has been discussed in several previous papers by the author (cf. Ref. 8). This coupling is evident in the basic force equations [Eq. (1)] and in the data in Fig. 2, both revealing that the engine performance is strongly angle-of-attack dependent.

The problematic flight-path response, noted in Ref. 15, for example, is associated with the washout of this response below the phugoid frequency. This makes flight path (or climb rate) difficult to control precisely. Reference 15 suggested that the problem is due to a low lift effectiveness Z_α, but our analysis indicates that perhaps the primary culprit is the high-flight velocity coupled with the altitude-dependent atmospheric density. For example, consider the case of slightly positive flight-path angle. With high velocity, a small positive flight path leads to a significant change in altitude and a concomitant reduction in atmospheric density. If the density is reduced, both thrust and lift are reduced. Hence, a positive flight path cannot be held indefinitely, either by increasing thrust or by pitching the vehicle. The bottom line from all this is that our system, with transfer matrix both unstable and nonminimum phase, is difficult or impossible to stabilize using the classical TECS architecture.

More specifically, the magnitudes of the $G(s)$ matrix elements defined earlier [Eq. (8)] are shown in Fig. 7. All data to follow are for a flight condition of Mach 8 at 85,000 ft; the stability-augmentation system in Fig. 6 is in place. The strong coupling, indicated by the magnitude of the off-diagonal elements relative to the diagonal, is clearly evident. Also, note that the $\dot{E}$ and the $\dot{ED}$ responses are almost equal, both for the thrust input and for the pitch control input. This is due to velocity dominating the total energy. These two essentially equivalent responses will be very difficult to control independently with these two inputs.

For the vehicle configuration being considered, flight-path angle is a much more preferable controlled response than energy distribution ED. This is true even though flight path is difficult to control, as already noted. Although precise control is impossible, we will show that sufficient control can be realized such that altitude can be controlled. Thus, consider selecting the response vector y now to be

$$y = \begin{bmatrix} \dot{E}/V = (\dot{V}/g) + \gamma \\ \gamma \end{bmatrix} \tag{9}$$

where energy distribution has been replaced by flight path. Shown in Fig. 8 are the magnitudes of the flight-path responses for the study vehicle (including the effect of stability augmentation). Considering Figs. 7 and 8, one can see that, although the dynamic coupling is still evident, these two responses ($\dot{E}/V$ and γ) are now significantly different. Furthermore, although still nonminimum phase, the transfer-function and transmission zeros of this 2×2 system are in much more advantageous locations than those with ED as a response. Hence, robust stabilization is facilitated.

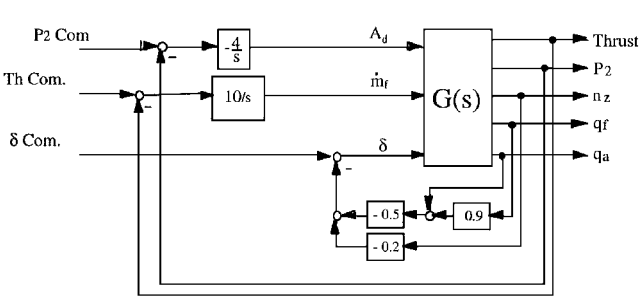

Fig. 6 Integrated inner-loop control law.

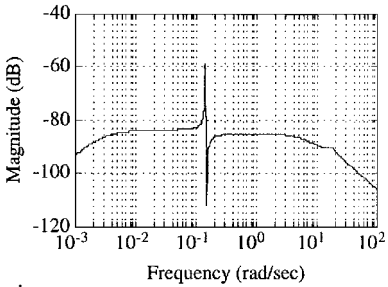

$(\dot{E}/V)/Th_c$

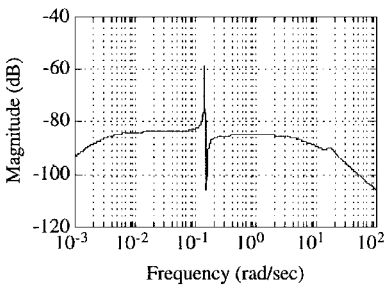

$(\dot{E}D/V)/Th_c$

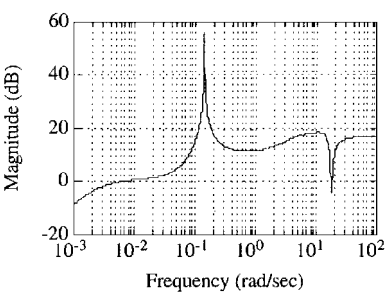

$(\dot{E}/V)/\delta_c$

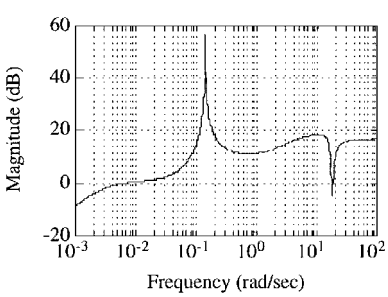

$(\dot{E}D/V)/\delta_c$

Fig. 7 Elements of transfer matrix $G(j\omega)$ [Eq. (8)], magnitudes only.

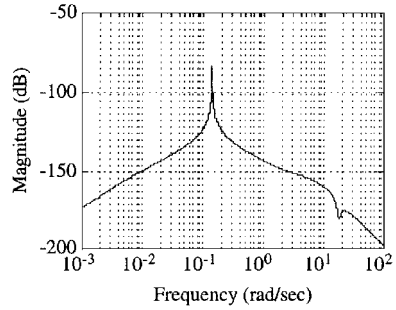

γ/Th_c

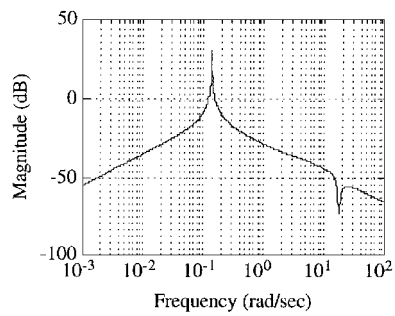

γ/δ_c

Fig. 8 Magnitudes of flight-path angle transfer functions.

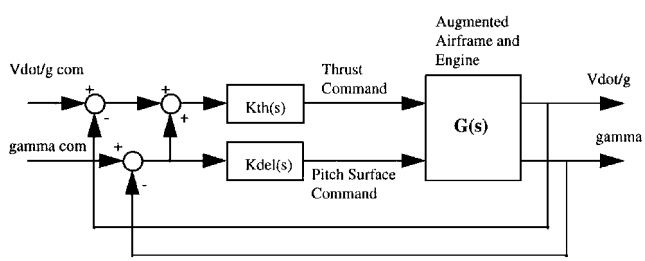

Fig. 9 Candidate SSTO guidance-law architecture, intermediate loop.

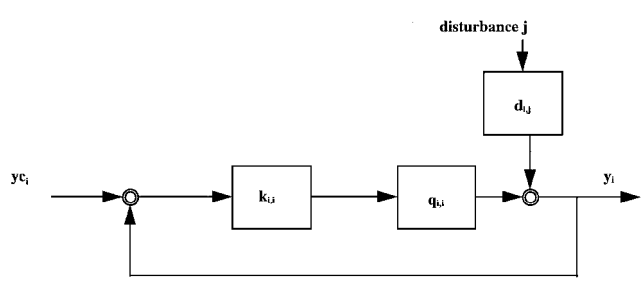

Fig. 10 Equivalent QFT loop.

The eigenvalues for this system [with outputs as in Eq. (9)] are $0.0001 \pm 0.140j$, -0.003, $-3.867 \pm 2.052j$, -10.085, $-3.178 \pm 16.109j$, and -28.08; and the transmission zeros are two at 0.0000, 3.092, -3.257, $-0.261 \pm 17.681j$, and -29.104.

With the feedback responses (E/V and γ) selected, compensation synthesis may now be addressed. Repeating for the sake of clarification, compensation for the system depicted in Fig. 9 is sought, where $G(s)$ is the 2×2 transfer matrix for the hypersonic vehicle (with stability augmentation), corresponding to the output vector in Eq. (9) and the control vector in Eq. (8).

Now if the corresponding $G(s)$ is written as

$$G(s) = \begin{bmatrix} g_{1,1} & g_{1,2} \\ g_{2,1} & g_{2,2} \end{bmatrix}$$

and $K(s)$ is the compensation matrix, the closed-loop system in Fig. 9 will be

$$y_{\mathrm{CL}}(s) = [I + GK]^{-1} GKP y_{\mathrm{com}}(s) = T_P(s) y_{\mathrm{com}}(s)$$

where P is a matrix of prefilters, taken as the identity in this discussion.

It can easily be shown[12–14] that, if $K(s)$ is diagonal, the complimentary sensitivity matrix for this system T_P may be written as

$$T_P(j\omega) = [\Lambda + K]^{-1}(KP - BT_P) \tag{10}$$

where

$$G^{-1} = H = [1/q_{i,j}] = \Lambda + B$$

$$\Lambda = \mathrm{diag}(h_{i,i}), \qquad B = \text{off-diag}(h_{i,j}), \quad i \neq j$$

and, therefore, the two elements on the diagonal of $K(s)$, $k_{1,1}$ and $k_{2,2}$, can be considered to be controlling four single-loop systems of the form depicted in Fig. 10. Under certain conditions,[12–14] these single-loop systems may be rendered to be, in the aggregate, equivalent to the original multivariable 2×2 system. One such condition guaranteeing equivalence can be achieved is a minimum-phase plant, which is not the case here. Another is that bounds on the

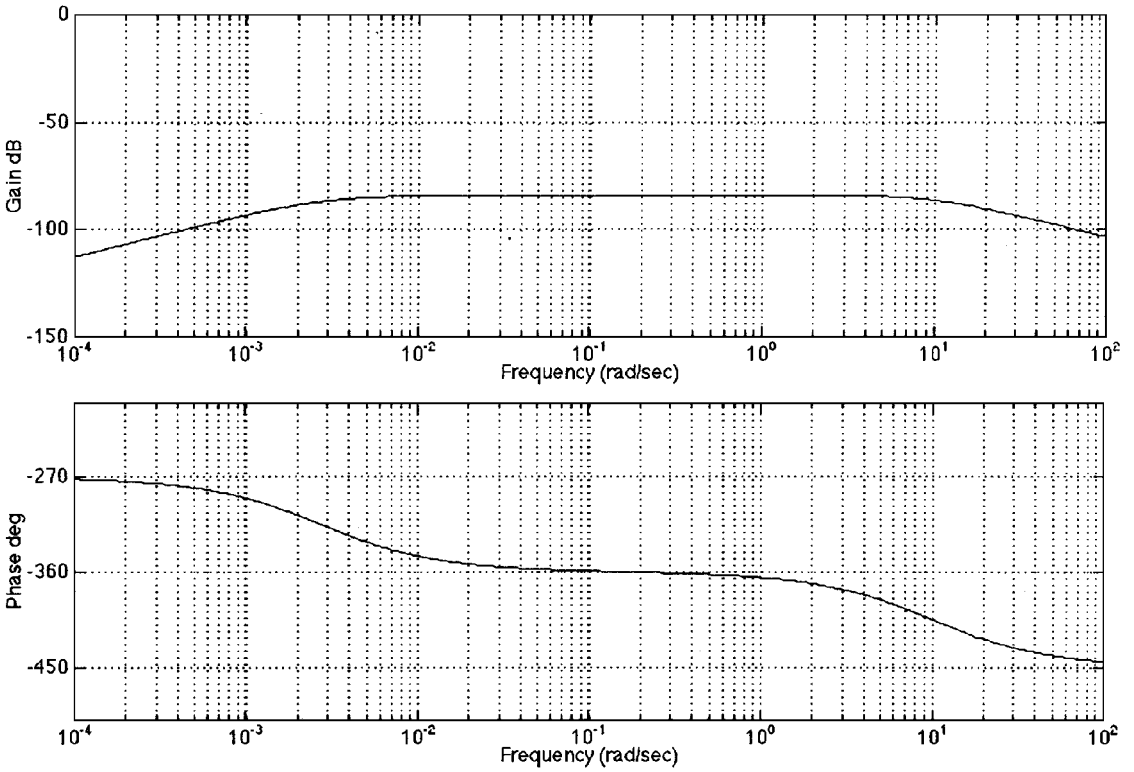

Fig. 11 Frequency response of $q_{1,1}$ [Eq. (11)].

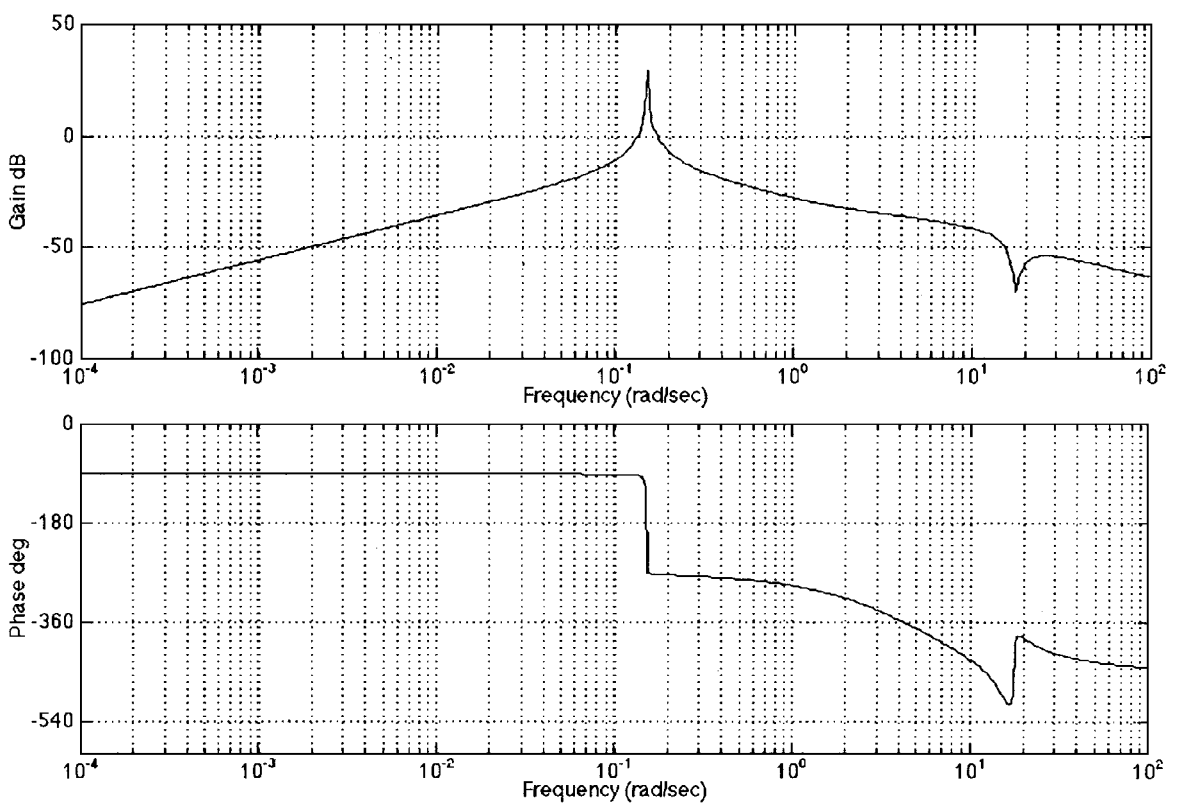

Fig. 12 Frequency response of $q^*_{2,2}$ [Eq. (12)].

magnitudes of the elements of the complementary-sensitivity matrix are known, which is not true in our case either. Therefore, though QFT will be used as a guide, it will not be used as the exact recipe for the synthesis.

Therefore, for the 2×2 system in question (again noting Figs. 9 and 10), we seek to determine $k_{1,1}$ and $k_{2,2}$, where

$$Th_c = k_{1,1}(s)[(\dot{V}_\varepsilon/g) + \gamma_\varepsilon], \qquad \delta_{\text{pitch}_c} = k_{2,2}(s)\gamma_\varepsilon$$

$$\gamma_\varepsilon = \gamma_c - \gamma \qquad \text{and} \qquad \dot{V}_\varepsilon = \dot{V}_c - \dot{V}$$

with

$$q_{1,1} = \frac{\det[G(j\omega)]}{g_{2,2}}$$

$$q_{2,2} = \frac{\det[G(j\omega)]}{g_{1,1}} \qquad \text{and} \qquad d_{i,j} = q_{i,i}h_{i,j}t_{Pj,i} \tag{11}$$

Because $G(s)$ is both open-loop unstable and nonminimum phase, extra care is required in the synthesis.[12,13] The $K(s)$ must successfully stabilize the closed-loop system, and just as with single-loop

systems, this requires some minimum closed-loop bandwidth. At the same time, the maximum bandwidth will be limited by the right-half-plane zero at 3.09 rad/s. And we have found that, to successfully apply QFT in this case, the technique of Ref. 13 should be used rather than that of Ref. 12.

The approach is to synthesize $k_{1,1}(s)$ first, using the given $q_{1,1}$, and then $k_{2,2}(s)$ is synthesized using the following effective plant:

$$q^*_{2,2} = g_{2,2} + \frac{k_{1,1}g_{1,2}g_{2,1}}{1 + k_{1,1}g_{1,1}} \tag{12}$$

rather than the $q_{2,2}$ given earlier in Eq. (11). This effective plant [Eq. (12)] includes $k_{1,1}(s)$ and can be found through simple block-diagram manipulation of the 2×2 system.

The frequency response of $q_{1,1}$ is shown in Fig. 11. These data suggest that, to achieve any kind of tracking performance, integral control will be required. The data also suggest that phase lead must be introduced near gain crossover. The following compensation meets this criterion and sets gain crossover at about 1 rad/s:

$$k_{1,1}(s) = \frac{20{,}000(s + 0.5)}{s} \text{lb}$$

Now consider the frequency response of $q^*_{2,2}$, shown in Fig. 12. These data also suggest that integral control will be required in $k_{2,2}$ and that phase lead is also necessary near gain crossover. Furthermore, gain crossover of this pitch-control loop must occur above the (unstable) phugoid frequency ($\sim$0.14 rad/s) yet below the zero at 3.09 rad/s. The data also suggest that stabilization of the system primarily results from closure of this pitch-control loop. The following meets this criterion:

$$k_{2,2}(s) = -\frac{20(s + 0.5)}{s}$$

Finally, investigation of the frequency responses of $d_{i,j}$ (not shown) reveals that the cross coupling in $G(s)$ will result in disturbances in each loop (see Fig. 10) out to the bandwidth of the closed-loop system, i.e., bandwidth of the $t_{i,j}$ from Eq. (10), or of the commanded inputs, e.g., γ_c, whichever is lower. These disturbances may be attenuated somewhat by using a prefilter P in Fig. 9, but that will not be addressed here.

The compensation as described sets the gain crossover frequency in both loops ($k_{1,1}q_{1,1}$ and $k_{2,2}q^*_{2,2}$) at 1 rad/s, stabilizes the system with good stability margins, and results in the following closed-loop eigenvalues: two at 0.0, -0.281, $-0.399 \pm 0.635j$, $-2.901 \pm 2.391j$, -18.271, $-3.774 \pm 16.372j$, and -28.602. Furthermore, it can be shown that this compensation makes the system's h/V-to-γ_c dynamics and the E/V-to-$(\mathrm{d}E/\mathrm{d}t)/V_c$ dynamics essentially k/s out to about 0.2 rad/s. Therefore, closing constant-gain loops around this system (as shown in Fig. 13), will deliver excellent stability margins. This completes the synthesis of the hierarchical multivariable guidance law.

Shown in Fig. 14 are step responses corresponding to a commanded change in total energy E of 6000 ft, with constant altitude, and a commanded change in altitude h of 1000 ft, with constant energy. Plotted are pitch rate and vertical acceleration, total control-surface deflection and fuel-flow rate, thrust, angle of attack, velocity, altitude, flight-path angle, and total specific energy E. Note that a change of total energy at constant altitude corresponds to simply a change in velocity. The controlled responses achieve their respective commanded values in about 10 s, all transients settle out in about 20 s, and the responses reveal good decoupling characteristics.

These simulation results were obtained using a small-perturbation model, linearized about the reference flight condition (Mach 8 and $h = 85{,}000$ ft). To implement the guidance law, the commanded velocity and acceleration used to generate the commands in Fig. 13 can be taken directly from the optimum velocity-altitude profile, such as that shown in Fig. 3. Any deviations from this trajectory then

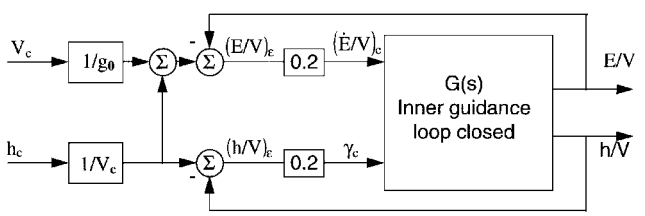

Fig. 13 Guidance law outer loop.

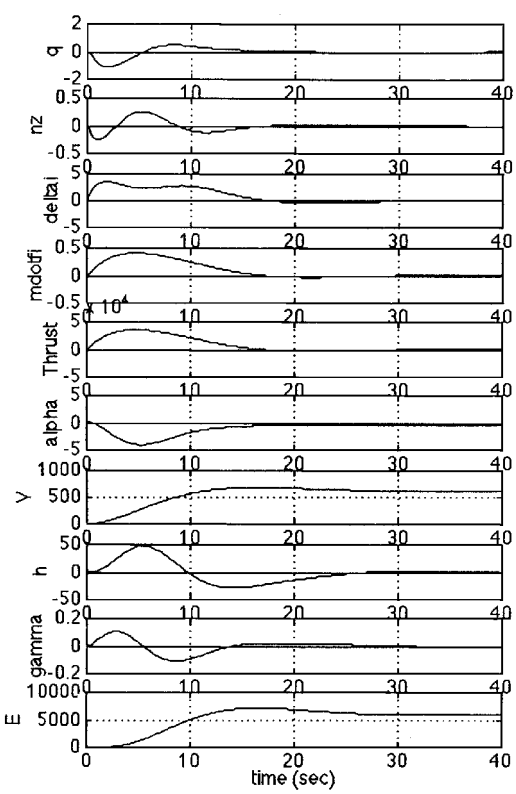

***E* step, 6000 ft**

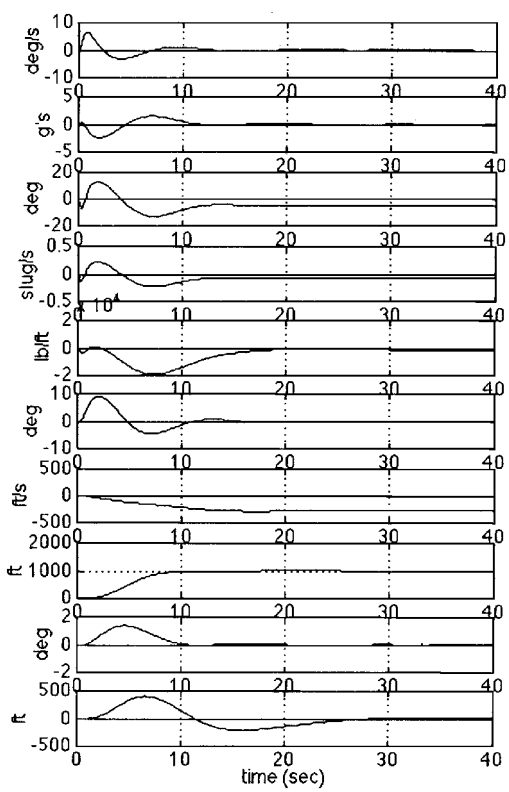

***h* step, 1000 ft**

Fig. 14 Guidance law step responses.

generate the energy-altitude errors to be regulated by the guidance law. Finally, gain scheduling may be required along the trajectory. But such gain scheduling would be modest if the trajectory reflected almost constant dynamic pressure, as is the case for the trajectory shown in Fig. 3.

Summary and Conclusions

The minimum-fuel ascent performance was evaluated for a generic airbreathing launch vehicle, and energy-state concepts were employed. Also, a hierarchical, multivariable guidance law was synthesized for following a prescribed optimal trajectory. The guidance-law synthesis approach also drew heavily from total-energy concepts, consistent with the performance analysis. Furthermore, the synthesis approach is consistent with QFT. Selection of the appropriate responses for feedback was shown to be critical, and the selected responses, energy and flight path, were chosen based on the unique characteristics of this vehicle. Namely, the responses are highly coupled, the total energy is dominated by velocity, the flight-path response is difficult to control, and the controlled plant is unstable and nonminimum phase. However, the synthesis technique yielded a simple, classical-looking feedback guidance law that successfully stabilized the system and appears to deliver very good performance.

Acknowledgments

This research is supported under NASA Langley Research Center Grant NAG1-1540. The author also wishes to acknowledge the contributions of Jon Velapoldi, Graduate Research Assistant in the Flight Dynamics and Control Laboratory, University of Maryland, who generated many of the numerical results presented.

References

[1]Corban, J. E., Calise, A. J., and Flandro, G. A., "Rapid Near-Optimal Aerospace Plane Trajectory Generation and Guidance," *Journal of Guidance, Control, and Dynamics*, Vol. 14, No. 6, 1991, pp. 1181–1190.

[2]Van Buren, M. A., and Mease, K. D., "Aerospace Plane Guidance Using Time-Scale Decomposition and Feedback Linearization," *Journal of Guidance, Control, and Dynamics*, Vol. 15, No. 5, 1992, pp. 1166–1174.

[3]Ardema, M. D., Bowles, J. V., and Whittaker, T., "Optimal Trajectories for Hypersonic Launch Vehicles," *Dynamics and Control*, Vol. 4, Kluwer Academic, Norwell, MA, 1994, pp. 337–347.

[4]Sachs, G., Bayer, R., Lederer, R., and Schaber, R., "Improvement of Aerospace Plane Performance by Overfueled Ramjet Combustion," *Zeitschrift für Flugwissenschaften und Weltraumforschung*, Vol. 17, 1993, pp. 25–32.

[5]Schmidt, D. K., and Lovell, T. A., "Mission Performance and Design Sensitivities of Air-Breathing Hypersonic Launch Vehicles," *Journal of Spacecraft and Rockets*, Vol. 34, No. 2, 1997, pp. 158–164.

[6]Schmidt, D. K., and Hermann, J. A., "The Use of Energy-State Analysis on a Generic Airbreathing Hypersonic Vehicle," *Journal of Guidance, Control, and Dynamics* (to be published); see also AIAA Paper 95-3372, Aug. 1995.

[7]Bryson, A. E., Desai, M. N., and Hoffman, W. C., "Energy-State Approximation in Performance Optimization of Supersonic Aircraft," *Journal of Aircraft*, Vol. 6, No. 6, 1969, p. 481.

[8]Schmidt, D. K., "Integrated Control of Hypersonic Vehicles," AIAA Paper 93-5091, Dec. 1993.

[9]Chavez, F. R., and Schmidt, D. K., "Analytical Aeropropulsive/Aeroelastic Hypersonic-Vehicle Model with Dynamic Analysis," *Journal of Guidance, Control, and Dynamics*, Vol. 17, No. 6, 1994, pp. 1308–1319.

[10]Hermann, J. A., "SSTO Mission Analysis of a Generic Hypersonic Vehicle," Final Rept., Flight Dynamics and Control Lab., Univ. of Maryland, College Park, MD, Aug. 1995.

[11]Lambregts, A. A., "Vertical Flight Path and Speed Control Autopilot Design Using Total Energy Principles," AIAA Paper 83-2239, Aug. 1983.

[12]Horowitz, I., "Quantitative Synthesis of Uncertain Multiple Input-Multiple Output Feedback Systems," *International Journal of Control*, Vol. 30, 1979, pp. 81–106.

[13]Horowitz, I., "Improved Design Technique for Uncertain Multiple-Input–Multiple-Output Feedback Systems," *International Journal of Control*, Vol. 36, 1982, pp. 977–988.

[14]Maciejowski, J. M., *Multivariable Feedback Design*, Addison–Wesley, Reading, MA, 1989, pp. 203–209.

[15]Thompson, P. M., Myers, T. T., and Suchomel, C., "Conventional Longitudinal Axis Autopilot Design for a Hypersonic Vehicle," AIAA Paper 95-4606, Aug. 1995.